J. Fluid Mech. (1999), *vol.* 395, *pp.* 181–209. Printed in the United Kingdom

On the gravitational displacement of three-dimensional fluid droplets from inclined solid surfaces

By P. DIMITRAKOPOULOS AND J. J. L. HIGDON

Department of Chemical Engineering, University of Illinois, Urbana, IL 61801, USA

(Received 23 September 1998 and in revised form 20 April 1999)

The yield conditions for the gravitational displacement of three-dimensional fluid droplets from inclined solid surfaces are studied through a series of numerical computations. The study considers both sessile and pendant droplets and includes interfacial forces with constant surface tension. An extensive study is conducted, covering a wide range of Bond numbers B_d, angles of inclination β and advancing and receding contact angles, θ_A and θ_R. This study seeks the optimal shape of the contact line which yields the maximum displacing force (or $B_T \equiv B_d \sin\beta$) for which a droplet can adhere to the surface. The yield conditions B_T are presented as functions of (B_d or $\beta, \theta_A, \Delta\theta$) where $\Delta\theta = \theta_A - \theta_R$ is the contact angle hysteresis. The solution of the optimization problem provides an upper bound for the yield condition for droplets on inclined solid surfaces. Additional constraints based on experimental observations are considered, and their effect on the yield condition is determined. The numerical solutions are based on the spectral boundary element method, incorporating a novel implementation of Newton's method for the determination of equilibrium free surfaces and an optimization algorithm which is combined with the Newton iteration to solve the nonlinear optimization problem. The numerical results are compared with asymptotic theories (Dussan V. & Chow 1983; Dussan V. 1985) and the useful range of these theories is identified. The normal component of the gravitational force $B_N \equiv B_d \cos\beta$ was found to have a weak effect on the displacement of sessile droplets and a strong effect on the displacement of pendant droplets, with qualitatively different results for sessile and pendant droplets.

1. Introduction

Fluid droplets adhering to inclined solid surfaces are encountered in several natural processes. Raindrops sticking to windowpanes and bubbles lining the inner surface of a glass of water are familiar examples. This phenomenon is also encountered in several engineering applications. Condensation of vapour onto a cool solid surface and the retention of pesticide sprays on plant leaves are typical examples. Depending on the nature of the process, we may want the droplets to remain attached to the solid surface or to be displaced. In both cases, it is important to identify the conditions under which a drop, attached to an inclined surface, will be displaced and slide down the surface (Dussan V. & Chow 1983).

The fundamental issues associated with gravitational displacement of droplets from inclined rigid boundaries have been addressed by Dussan V. and coworkers (Dussan V. & Chow 1983; Dussan V. 1985). These authors developed yield criteria for the critical Bond number B_d as a function of the advancing and receding contact angles, θ_A and θ_R,

and the angle of inclination β. In the first paper, the analysis was based on asymptotic theory valid for small advancing contact angles θ_A and much smaller contact angle hysteresis $(\theta_A - \theta_R)$. In the second paper the asymptotic theory is less restricted and is valid for small contact angle hysteresis $(\theta_A - \theta_R)$ and Bond number B_d but for any advancing contact angle θ_A. In both papers, a contact line with two parallel sides along the direction of inclination was assumed. This shape is usually observed when the drop has been displaced and slides down the surface (Bikerman 1950; Furmidge 1962), but is not observed prior to displacement (Rotenberg, Boruvka & Neumann 1984; Extrand & Kumagai 1995). Although both theories have assumed that $\theta_A - \theta_R$ is small, we note that the hysteresis may in fact be quite large. Values of $\theta_A - \theta_R$ in the range of 20°–30° have been routinely reported for gas–liquid systems, while substantially higher values may occur for liquid–liquid systems (Good & Koo 1979; Good 1979). Further discussion and references on contact angle hysteresis have been given in our paper on the displacement of two-dimensional fluid droplets due to the action of a viscous shear flow (Dimitrakopoulos & Higdon 1997, hereafter referred to as DH1).

In the area of computational studies on drop displacement, Brown, Orr & Scriven (1980) modelled the problem of deformation of a drop of a given volume and density on an inclined plane. They used a Newton/Galerkin finite element method to solve the Young–Laplace equation, and calculated the drop shape for several inclination angles β. Milinazzo & Shinbrot (1988) studied the similar problem of a drop deformation on a vertical wall as the Bond number B_d increases from zero. They conducted a detailed study, covering initial shapes with a wide range of contact angles. In both papers, the authors assumed a contact line of fixed circular shape, and solved for the distribution of the contact angles around the contact line. The prescription of fixed circular contact lines is an approximation which does not conform to experimental observations. Tuck & Schwartz (1991) considered two- and three-dimensional thin droplets on inclined surfaces, while the drop perimeter was required to lie on a given closed curve.

In the present article, we consider the displacement of a three-dimensional fluid droplet from an inclined plane substrate due to the action of gravity. Our goal is to provide a comprehensive solution of the problem and hence to determine the effects of all the relevant parameters and to assess the limits of the asymptotic theories. We consider both sessile $(0° \leqslant \beta \leqslant 90°)$ and pendant $(90° \leqslant \beta \leqslant 180°)$ droplets, with arbitrary values for the Bond number B_d, the advancing contact angle θ_A and the contact angle hysteresis $(\theta_A - \theta_R)$. We seek the optimal shape of the contact line C which gives the maximum displacing force for which a droplet can adhere to the surface. This critical displacing force gives the yield condition for the droplet and is determined as a function of the contact angle θ_A and hysteresis $(\theta_A - \theta_R)$.

To address the problem of drop displacement, we employ a novel, three-dimensional Newton method to determine the equilibrium shape of fluid interfaces and an optimization technique which is combined with the Newton iteration to solve for the optimal shape of the contact line. Both methods are presented in our recent paper on the displacement of three-dimensional fluid droplets in low-Reynolds-number shear flows (Dimitrakopoulos & Higdon 1998, hereafter referred to as DH2) and will not be discussed in detail in the present paper.

2. Mathematical formulation

We consider a three-dimensional droplet attached to an inclined solid plane as illustrated in figure 1. The droplet size is specified by its volume V_0 or equivalently by the radius a of a spherical droplet of volume $V_0 = (4\pi/3)a^3$. The droplet (fluid 1) has

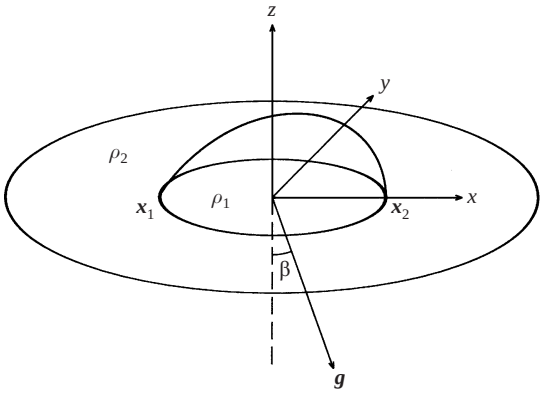

FIGURE 1. Fluid droplet attached to an inclined solid boundary.

density ρ_1, while the surrounding fluid has density ρ_2. The gravitational acceleration is g and the gravity vector forms an angle β with respect to the negative z-direction; hence β is the angle of inclination of the plane substrate. The surface tension γ is assumed constant. The contact line forms a closed curve C in the (x, y)-plane which intersects the x-axis at two points, with the higher point and contact angle designated $\boldsymbol{x}_1$ and θ_1, and the corresponding lower values $\boldsymbol{x}_2$ and θ_2.

The Bond number B_d, representing the ratio of the gravitational forces to interfacial forces, is defined by

$$B_d = \frac{(\rho_1 - \rho_2)ga^2}{\gamma}.$$

The calculation of equilibrium shapes for fluid interfaces in the presence of gravity may be formulated as a problem of fluid statics where the jump in hydrostatic pressure at the interface matches the pressure jump associated with surface tension. At the interface, the boundary condition on the surface stress $\boldsymbol{f}$ is

$$\Delta \boldsymbol{f} = \boldsymbol{f}_2 - \boldsymbol{f}_1 = \gamma(\nabla \cdot \boldsymbol{n})\boldsymbol{n} + (\rho_2 - \rho_1)(\boldsymbol{g} \cdot \boldsymbol{x})\boldsymbol{n}, \tag{1}$$

where $\boldsymbol{n}$ is the unit normal which we choose to point into fluid 2.

For droplets in contact with a solid boundary, additional conditions are required to prescribe the interface shape in the vicinity of the contact line. For real surfaces (i.e. rough and chemically inhomogeneous), it has been found that the static contact angle exhibits a hysteresis effect where the contact line remains stationary for any angle in the range

$$\theta_R \leqslant \theta \leqslant \theta_A. \tag{2}$$

The limits θ_A and θ_R are called the advancing and receding angles respectively. As in DH2, we assume that the advancing and receding angles θ_A and θ_R are physical constants and require that (2) hold for all angles along the contact line C. More details and references concerning the phenomenon of contact angle hysteresis as well as the boundary conditions along the contact line can be found in our earlier papers (DH1, DH2).

With the interfacial and contact line boundary conditions given above, the determination of the critical conditions for drop displacement may be formulated as an optimization problem. This problem may be stated as follows: for a given contact angle θ_A and hysteresis $\theta_A - \theta_R$, find that configuration corresponding to the highest Bond number B_d for which an equilibrium solution exists. An alternative, but equiv-

alent, problem may be stated: for a given contact angle θ_A and Bond number B_d, find that configuration corresponding to the minimum $\theta_A - \theta_R$ for which an equilibrium solution exists. This latter form proves more convenient for numerical computations and has been adopted in the present work; however, the results may be viewed in either context with equal validity. The optimization problem may be stated formally as:

$$\text{for fixed } \theta_A \text{ and } B_d, \text{ search over all contact lines } C, \text{ to minimize } \ \theta_A - \theta_R \tag{3}$$

subject to

$$\theta_i \leqslant \theta_A, \tag{4}$$

$$\theta_i \geqslant \theta_R, \tag{5}$$

$$\boldsymbol{x}_1 \equiv \text{fixed} \tag{6}$$

for interface configurations satisfying the boundary condition (1)

with a hydrostatic pressure distribution.

Here θ_i, $i = 1, \ldots, N_{cl}$ are the contact angles along the contact line C, and N_{cl} is the number of discrete points specifying the position of the contact line.

The solution to this optimization problem gives the critical condition for drop displacement in terms of the maximum Bond number B_d or minimum contact angle hysteresis $\theta_A - \theta_R$. Unfortunately, the optimal configuration and yield condition may not always be realized in an experiment. In any experiment, the droplet starts with a specified initial configuration and goes through a progression of different configurations as the experimental conditions (e.g droplet size, or substrate inclination angle) are changed. The conditions of the experiment may be such that the droplet cannot reach the optimal equilibrium configuration and will be displaced at less extreme values of the parameters.

To test the sensitivity of the yield conditions to the experimental procedure, we consider one additional optimization problem. In many experiments, the droplet shape becomes elongated in the x-direction, i.e. in the direction parallel to the component of gravity in the plane of the wall. To determine the critical yield conditions in such experiments, we reformulate the optimization problem above with the additional constraint that the magnitude of the lateral positions y cannot exceed the maximum value $|y_0^{max}|$ in the initial configuration of the droplet. The constraint on the y-position adds the following inequality constraint to the optimization problem:

$$-|y_0^{max}| \leqslant y_i \leqslant |y_0^{max}|, \quad i = 1, \ldots, N_{cl}. \tag{7}$$

This optimization will be called the *y-constrained* optimization problem while the previous problem will be called the *unconstrained* optimization problem.

The optimization problems described above may be solved by a number of different approaches. As an example, for a given contact line C, one might use finite element methods to solve the Young–Laplace equation for the interface shape and thereby to determine the contact angles (Brown *et al.* 1980). The solution procedure for a given C might be combined with nonlinear programming methods to solve the full optimization problem. In the present paper, we have adopted a different approach. In our earlier work (DH2), we developed algorithms to solve optimization problems similar to those above for droplets immersed in viscous flows governed by the Stokes equations. The quiescent fluid and hydrostatic pressure fields arising in the present work may be viewed as a trivial case of Stokes flow with zero velocity. Under these conditions, the algorithms of the earlier effort may be employed without modification,

yielding solutions of the optimization problem for the interface shapes and contact angles. It should be emphasized that the rationale for this approach is the pre-existence of a general algorithm for solving the interfacial optimization problems in the presence of arbitrary Stokes flows.

A detailed description of our numerical methods for the Stokes flow problem has been given in DH2. Briefly, the method employs a spectral boundary element algorithm to solve the Stokes equations, a Newton iteration to determine the interface shape, and a successive linear programming algorithm to solve the optimization problem. In the present work, the numerical discretization of the boundary surfaces as well as the order of the spectral approximations are the same as described in DH2, § 3. The present problem admits one level of symmetry around the plane $y = 0$, which we exploit to reduce the computational time and memory requirements. Detailed tests of the numerical algorithm were described in DH2. We note that additional comparisons for the gravitational problem have been made with the results of Brown *et al.* (1980) (their figure 5) and Milinazzo & Shinbrot (1988) (their figure 20), for the case of circular contact lines. Our computations are in excellent agreement with these earlier results.

3. Results

In this paper, our goal is to present a comprehensive study of the problem of gravitational displacement of fluid droplets from solid surfaces. The relevant parameters are the Bond number B_d, the inclination angle β, the advancing contact angle θ_A and the receding contact angle θ_R or equivalently the hysteresis $\theta_A - \theta_R$. The gravitational displacement force may be characterized by its tangential and normal components relative to the plane substrate: $B_T \equiv B_d \sin\beta$ and $B_N \equiv B_d \cos\beta$. Alternatively, we may consider the total Bond number B_d and the inclination angle β. We shall see that the force components (B_T, B_N) are the most relevant parameters for interpreting the physics of gravitational displacement; however, the combination (B_d, β) most closely represents the conditions of experimental systems.

For convenience, we assume that the density of the droplet is greater than that of the surrounding fluid. With this assumption, the Bond number is always positive. For inclination angles $0^\circ \leqslant \beta \leqslant 90^\circ$, the normal force is positive ($B_N \geqslant 0$) and acts to flatten the droplet against the solid. For inclination angles $90^\circ \leqslant \beta \leqslant 180^\circ$, the normal force is negative ($B_N \leqslant 0$) and acts to pull the droplet away from the solid. Results for droplets (or bubbles) with density less than the surrounding fluid may be obtained by reversing the densities and replacing β with $180^\circ - \beta$.

We note that there are two common scenarios which may be encountered in experiments or applications. In the first scenario, one has a surface at a fixed inclination angle β, and the volume (or B_d) of the droplet is increased until the droplet is displaced. This system is associated with applications involving dropwise condensation or experiments in which the volume of the droplet is increased by injecting fluid. In the second scenario, a droplet of fixed volume (or B_d) is placed on a horizontal surface, and the plane is tilted until the critical angle of inclination β is reached. This system is favoured in many experiments designed to measure contact angle hysteresis. For our purposes, the first scenario involves increasing the Bond number while holding β constant, while the second involves varying β while holding B_d constant. The details of the experimental procedure have no effect on the prediction of the yield condition for the unconstrained optimization problem. However, in our discussion of the *y-constrained* optimization, we shall see that the experimental procedure may have a subtle effect on the observed experimental results.

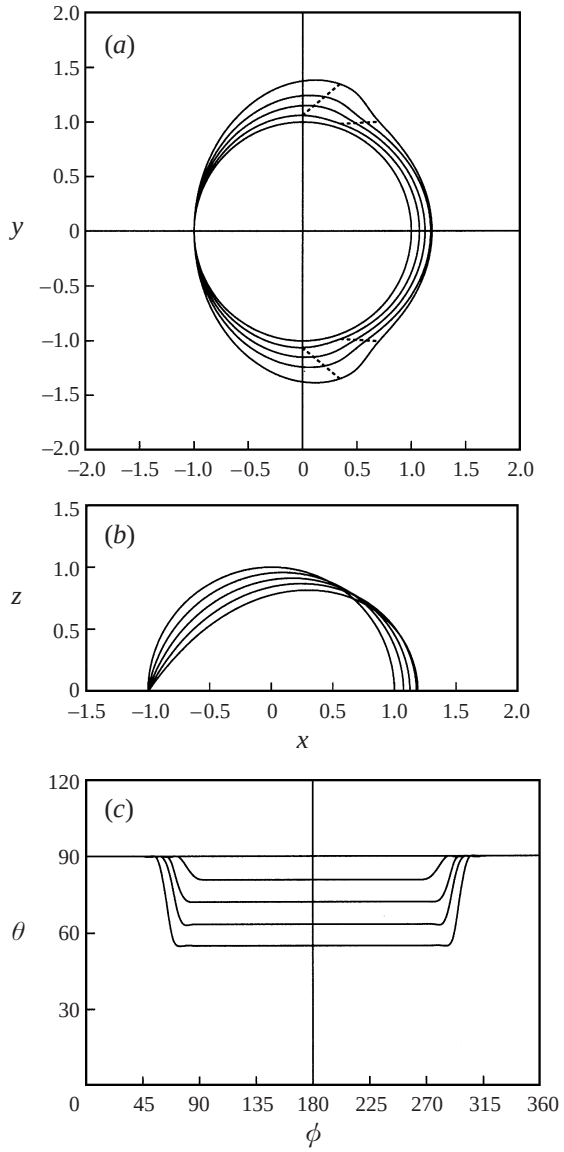

FIGURE 2 (*a–c*). For caption see facing page.

With this overview, we present a brief outline of the results in the subsections below. In the first three subsections, the yield condition is determined as a function of the contact angle hysteresis $\theta_A - \theta_R$ for droplets with different contact angles θ_A. Section 3.1 provides results for vertical walls, while § 3.2 covers inclined walls with sessile droplets ($0^\circ \leqslant \beta \leqslant 90^\circ$) and § 3.3 covers inclined walls with pendant droplets ($90^\circ \leqslant \beta \leqslant 180^\circ$). In § 3.4, we consider the second experimental scenario by fixing the Bond number and varying the inclination angle until the yield condition is reached. Finally, in § 3.5 we compare our computational results with experimental observations and theoretical predictions.

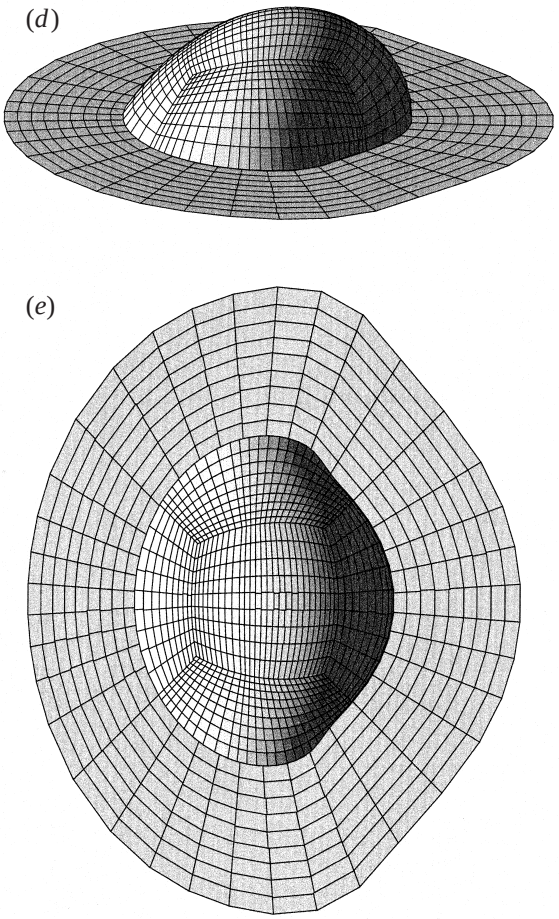

FIGURE 2. Equilibrium shapes for droplets on a vertical wall ($\beta = 90^\circ$) with advancing contact angle $\theta_A = 90^\circ$ and for the unconstrained optimization problem. For (*a–c*) the Bond number is $B_d = 0$, 0.1, 0.2, 0.3, 0.4. (*a*) The optimal shape of the contact line. The dashed lines show the location of the jump region. (*b*) The cross-section of the drop surface with the plane $y = 0$. (*c*) The variation of the contact angle θ as a function of the azimuthal angle ϕ. (*d,e*) The drop surface for Bond number $B_d = 0.4$.

3.1. *Drop displacement on a vertical wall,* $\beta = 90^\circ$

We begin our investigation of the gravitational displacement problem by considering a fluid droplet on a vertical wall ($\beta = 90^\circ$). In this case the normal component of the gravitational force B_N is zero, and the total gravity force acts in the positive x-direction, parallel to the solid surface. Figure 2(*a,b*) shows the optimal shapes of the contact line and the drop profiles (i.e. the cross-section of the drop surface with the plane $y = 0$) for the unconstrained optimization for a drop with advancing contact angle $\theta_A = 90^\circ$ and for several values of the Bond number B_d.

With each successive curve, a larger B_d is specified, and a larger contact angle hysteresis is required to hold the drop in place. The distribution of contact angles around the contact lines are shown in figure 2(*c*), while figure 2(*d,e*) shows three-dimensional views for a typical droplet shape. Two noteworthy features are apparent from these figures. First (see figure 2*a*), we observe that the lower edge of the contact line is continuously displaced further downward as the Bond number is increased. As the gravitational force on the droplet increases, the net interfacial force must be

increased, and this is achieved by reducing the contact angle on the front of the droplet. With a smaller angle, the droplet spreads over a larger area to accommodate the same fluid volume. The second noteworthy feature is that the width of the contact line in the y-direction increases as the Bond number is increased. This feature is of interest for a number of reasons. On first impression, it would seem more likely that a droplet should spread in the x-direction (parallel to gravity), and not in the y-direction; however, a simple physical argument reveals the logic of this transition. If a droplet spreads in the x-direction, the long sides of the drop yield interfacial forces at the contact line which pull sideways and do not act to counter the gravitational force. By contrast, if the droplet spreads in the y-direction, the increased width of the contact line on the front and back increases the net interfacial force which is proportional to $\theta_A - \theta_R$ multiplied by the width. The increased width and the reduced contact angle both act to increase the interfacial force. Thus the most stable drop for a given volume has the wide asymmetrical profile illustrated in figure 2 (a). While the contours seen in these figures represent the optimal (most stable) contact lines a droplet may achieve, they are not necessarily the contours which will be seen in an experiment when a droplet is placed on a horizontal surface, and the surface is tilted. We shall return to this issue in the discussion below. It is worth noting that these shapes are similar to the equilibrium shapes for a droplet immersed in a viscous shear flow (DH2, figure 4a).

While we have focused on the shape of the contact line, the variation of the contact angle around the contour also has an important effect on the force balance. Figure 2 (c) shows the variation of the contact angle θ along the contact line as a function of the azimuthal angle ϕ for the stated values of θ_A and B_d. The azimuthal angle ϕ is measured with respect to the positive x-direction as usual. This figure shows that the lower portion of the contact line admits a single maximum contact angle (the advancing angle θ_A) while its upper portion admits a single minimum angle (the receding angle θ_R). Between these two portions there is an acute jump in the distribution of the contact angles which occurs for $\phi \approx 55^\circ$–90° and $\phi \approx 270^\circ$–305°. These locations are noted as dashed lines on the contact line contours in figure 2 (a). Clearly, the portion of the contact line which admits the advancing angle θ_A is smaller than the portion which admits the receding angle θ_R. The rapid jump in contact angle is a further consequence of the droplet's attempts to maximize the interfacial force. The drop holds the minimum contact angle over the entire upper portion of the contact line, then makes the fastest possible transition to the maximum angle on the lower portion of the contour. The rapid change in contact angle observed here is in distinct contrast to the smooth distribution observed in simulations for circular contact lines (Milinazzo & Shinbrot 1988; Brown *et al.* 1980). Finally, with reference to the numerical computations, we note that this jump presents a significant challenge to the numerical algorithm. As indicated in DH2 (§ 3), it is important to concentrate grid points near the jump to accurately capture the rapid change in the interfacial shape.

Having explored the basic principles associated with the deformation and displacement of the droplet, we turn our attention to the prediction of the yield conditions as a function of the drop parameters. Figure 3 shows the critical B_d as a function of hysteresis $\theta_A - \theta_R$ for a drop on a vertical wall ($\beta = 90^\circ$), for several values of θ_A. For each point on a given curve, we specify the Bond number and a fixed value of θ_A, and then find the optimal shape which requires the minimum hysteresis $\theta_A - \theta_R$ for equilibrium. The specified B_d then represents the yield condition for that value of θ_A and $\theta_A - \theta_R$. The terminal points at the end of each curve represent the largest $\theta_A - \theta_R$ for which accurate numerical calculations could be executed. The criteria for an accurate numerical solution include convergence of the linear programming iteration and of the Newton iteration and consistency with increasing order of the spectral

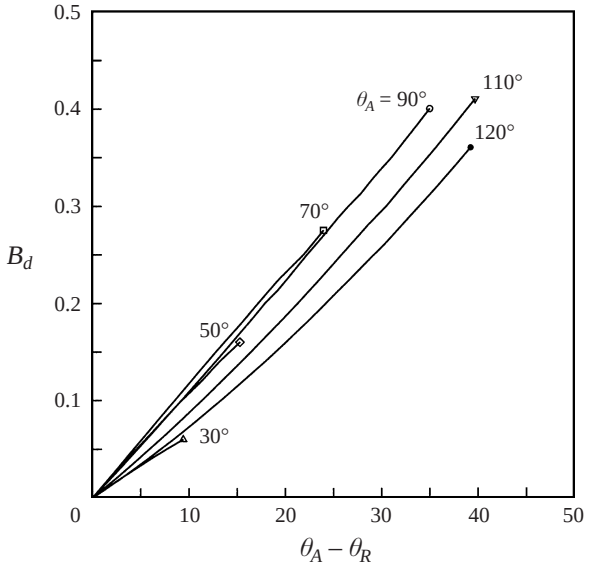

FIGURE 3. Critical Bond number B_d versus hysteresis $\theta_A - \theta_R$ for $\beta = 90°$ and for the unconstrained optimization problem.

expansion. For all cases, we find that the algorithm stops owing to the convergence failure of the linear programming algorithm. On physical grounds, it appears that the true terminal point of each curve corresponds to a value $(\theta_A - \theta_R) \to \theta_A$, for which $\theta_R \to 0$ and the interface becomes tangent to the boundary wall on the upper portion of the contact line. We emphasize that figure 3 gives accurate yield conditions for the plotted parameter values. The only limitation is that we are unable to provide precise predictions for extreme values of the hysteresis $\theta_A - \theta_R$.

The curves of figure 3 reveal interesting behaviour for the critical B_d at different advancing contact angles θ_A. For a given hysteresis $\theta_A - \theta_R$, increasing the contact angle θ_A from small values, *increases* the critical gravitational force or B_d, for values of the advancing contact angle up to $\theta_A \approx 70°$. Above this value, increasing the contact angle θ_A *decreases* the critical Bond number. Figure 3 shows that the critical Bond number B_d for $\theta_A = 90°$ is close to that for $\theta_A = 70°$, but admits a much smaller value at $\theta_A = 110°$ and $\theta_A = 120°$. It is of interest to note that Dussan V. (1985) found the same behaviour (her figure 6), for the case of small hysteresis $\theta_A - \theta_R$ and Bond number B_d.

The explanation for the behaviour as a function of contact angle θ_A is straightforward when one considers the force balance on the droplet. The displacing force is determined by the weight of the droplet and the angle of inclination, i.e. $(\rho_1 - \rho_2)V_0 g \sin\beta$, which is equal to $(4\pi/3)(\rho_1 - \rho_2)a^3 g \sin\beta$. For small hysteresis, the net interfacial force is proportional to the width of the droplet (or radius r of the contact line) and the quantity $(\cos\theta_R - \cos\theta_A)$ which measures the component of the force parallel to the wall. The radius of the contact line decreases monotonically with θ_A, while the quantity $(\cos\theta_R - \cos\theta_A)$ scales as $(\theta_A - \theta_R)\sin\theta_A$ for small hysteresis. It increases for small θ_A but reaches a maximum at $\theta_A = 90°$. All scalings to this point are valid for arbitrary contact angle θ_A. For small contact angles, the decrease in the contact line radius scales as $\sim {\theta_A}^{-1/3}$ and is more than offset by the increase in $\sin\theta_A$ ($\sim \theta_A$); the interfacial force increases, and hence a stronger displacement force is required with scaling $B_d \sim {\theta_A}^{2/3}$. For larger contact angles, the radius of the contact line decreases slowly but monotonically, while $\sin\theta_A$ approaches its maximum value. At angles slightly below $\theta_A = 90°$, the effect of the reducing radius becomes dominant, and the interfacial

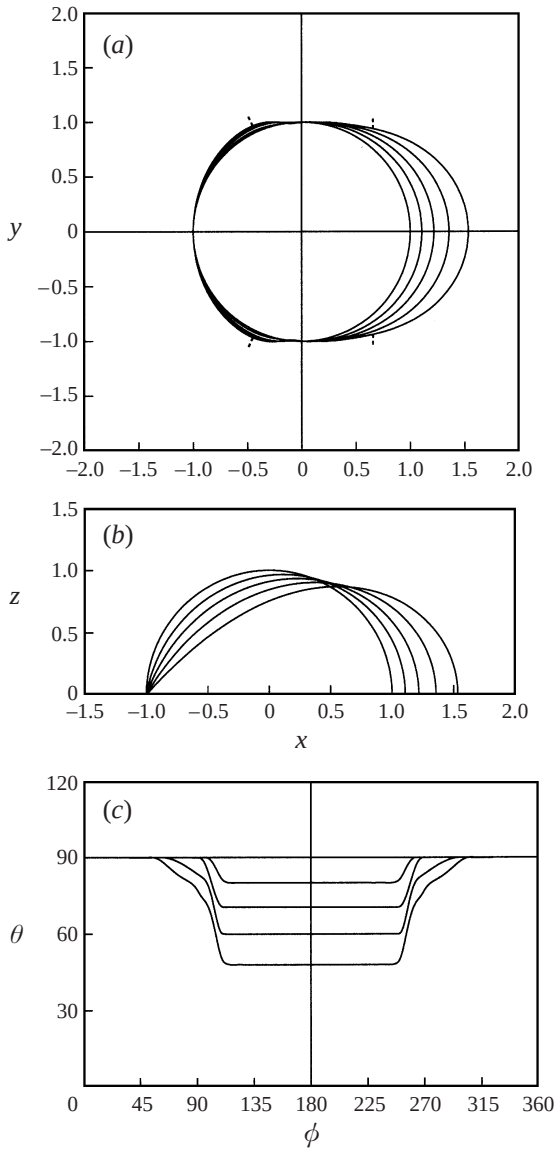

FIGURE 4 (*a–c*). For caption see facing page.

force begins to decrease. For angles above $\theta_A = 90°$, both the radius and the $\sin\theta_A$ term decrease as θ_A increases. Thus the critical Bond number reaches a maximum at $\theta_A \approx 70°$ and decreases for higher angles with more rapid decrease above 90°.

At this time, we return to the subject of the contact line contours and consider how the conditions of an experiment might affect the observed shapes. Recall that the solutions presented in figure 2 (*a*) represent optimal solutions independent of the initial configuration of a droplet. Consider a droplet with hysteresis $\theta_A - \theta_R$. On a horizontal surface, this droplet may exist in an infinite number of configurations. If the droplet is formed by injecting liquid through a small hole in the substrate, it might form a section of a sphere with all contact angles having the value θ_A. Upon the tilt of the surface, the lower portion of the contact line would immediately begin to move downwards as the value of θ_A is exceeded. This would lead to elongated droplets with

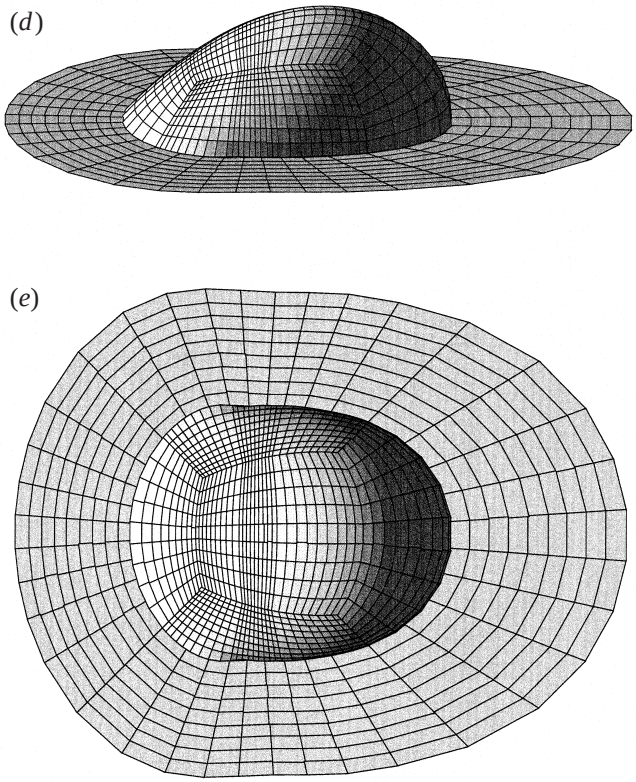

FIGURE 4. Equilibrium shapes for droplets on a vertical wall ($\beta = 90^\circ$) with advancing contact angle $\theta_A = 90^\circ$ and for the y-constrained optimization problem. For (a–c) the Bond number is $B_d = 0$, 0.1, 0.2, 0.3, 0.4. (a) The shape of the contact line. The small dashed lines show the jump region for $B_d = 0.4$. (b) Drop profile. (c) The variation of the contact angle θ as a function of the azimuthal angle ϕ. (d,e) The drop surface for Bond number $B_d = 0.4$.

shapes quite different from those shown in figure 2. The yield condition for these droplets may be less than for those with the optimal contours of figure 2. In another experiment, suppose one starts with the droplet on a horizontal surface as before, but extracts fluid until the drop just begins to recede, yielding a section of sphere with all contact angles equal to θ_R. When the surface is tilted, it is the upper portion of the droplet which will move first as the contact angle falls below θ_R. In this case, short wide droplets will form whose shape might well approach the optimal shapes shown above. The important conclusion here is that the actual yield condition is determined not only by the maximum possible yield condition, but also by the initial configuration of the droplet, the conditions of the experiment and the evolution of the contact line.

To test the sensitivity of the critical gravitational force subject to these conditions, we consider the *y-constrained* optimization problem. As noted in the previous section, for this problem, we assume that the experimental conditions constrain the droplet to move in the direction of gravity, and we require that the y-positions do not exceed the maximum extension in the initial configuration. In this subsection, as well as in § 3.2 and § 3.3 below, the undisturbed drop shape corresponds to $B_d = 0$ and thus it is a spherical cap with a single angle θ_A around a circular contact line.

Figure 4 (a,b) shows the contact line contours and the drop profiles for the y-constrained optimization for a droplet with advancing contact angle $\theta_A = 90^\circ$ and for

several values of the Bond number B_d. As with the unconstrained optimization above, on each successive curve, a larger B_d is specified and a larger contact angle hysteresis is required to hold the drop in place. Figure 4(*a*) shows that the lower portion of the contact line has been displaced much further downwards compared with that of the unconstrained optimal problem for the same values of the Bond number. This behaviour is to be expected because of the y-constraint on the shape of the contact line. These contact line contours are qualitatively similar to the experimental shapes reported by Extrand & Kumagai (1995) (their figure 3) and Rotenberg *et al.* (1984) (their figure 8).

Figure 4(*c*) shows the variation of the contact angle θ along the y-constrained contact line as a function of the azimuthal angle ϕ for the prescribed values of θ_A and B_d. As before, the lower portion of the contact line admits a single maximum contact angle θ_A, its upper portion admits a single minimum contact angle θ_R, and there is an acute jump in the distribution of the contact angles which occurs for $\phi \approx 55^\circ$–115° and $\phi \approx 245^\circ$–305°. The positions of the contact line, at which the jump occurs for $B_d = 0.4$, are noted in figure 4(*a*). In contrast to the unconstrained contact line, the portion of the y-constrained contact line which admits the advancing angle θ_A is larger than the portion which admits the receding angle θ_R. In comparing figures 2(*c*) and 4(*c*) for the same Bond number, it is obvious that the y-constrained contact line admits a smaller receding contact angle θ_R. This implies that the droplet requires more hysteresis to hold its position, i.e. that it is slightly less stable than the optimal solution. Figure 4(*d*,*e*) shows two three-dimensional views of the drop for $B_d = 0.4$ for this problem. Comparison with the three-dimensional views in figure 2 shows the obvious differences between the drop shapes for the two optimization problems. The influence of the advancing contact angle θ_A on the y-constrained droplet is qualitatively similar to the unconstrained case (shown in figure 3). Detailed results for this case are given in Dimitrakopoulos (1998).

For a direct comparison between the unconstrained and y-constrained optimizations, we show the critical Bond number for the two cases on the same plot in figure 5 for both a large contact angle $\theta_A = 90^\circ$ and a smaller angle $\theta_A = 30^\circ$. In each of these figures, we plot one additional curve, corresponding to the case of a circular contact line. This last curve is determined as the solution of an optimization problem for contact lines of circular shape but arbitrary radius (DH2, § 2.3). The insets in each figure show examples of the actual shape of the contact line contours and the drop profiles for the three different optimization problems. The results plotted in figure 5 show that for large advancing contact angles θ_A, the critical Bond number B_d for the unconstrained optimization problem is higher than for the two other problems as expected. As the contact angle θ_A decreases, the difference in B_d for the unconstrained and the y-constrained problem becomes smaller and smaller. (Note the different scales in the figures 5*a* and 5*b*.) For all angles θ_A studied, we found that the circular contact line admits a significantly smaller Bond number. For a droplet free to move over a solid surface, these results show that the assumption of a circular contact line predicts a measurably smaller yield stress than would be achieved in practice.

3.2. *Displacement of a sessile drop*, $0^\circ \leqslant \beta \leqslant 90^\circ$

Having considered the influence of the Bond number B_d on the displacement of a drop on a vertical wall, we now turn our attention to the effects of the inclination angle β. We begin by considering a sessile drop, i.e. $0^\circ \leqslant \beta \leqslant 90^\circ$. In figure 6(*a*) we plot the critical B_d as a function of hysteresis $\theta_A - \theta_R$ for a drop with $\theta_A = 90^\circ$, for the unconstrained optimization problem and for several angles of inclination β in the

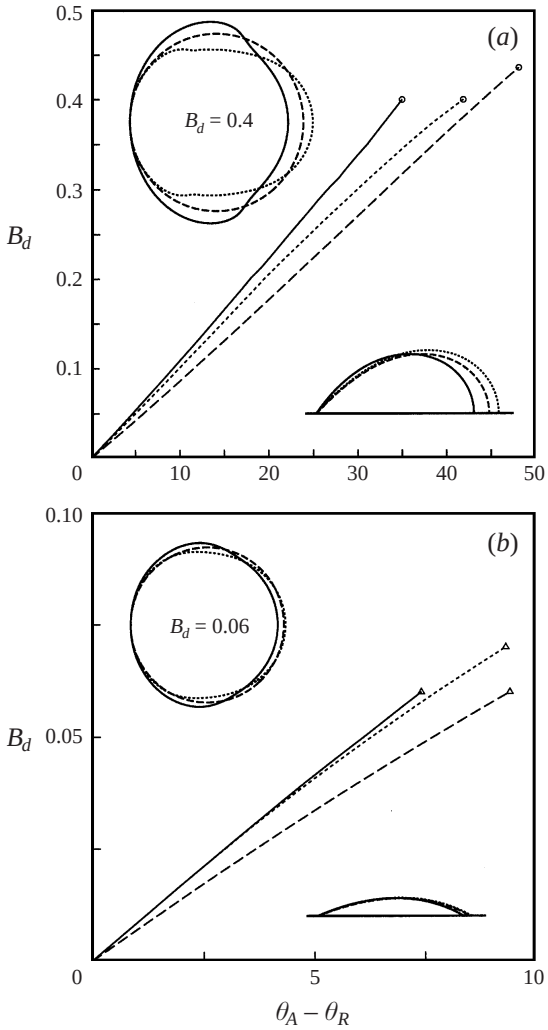

FIGURE 5. Influence of the shape of the contact line for droplets on a vertical wall ($\beta = 90°$). (*a*) Critical Bond number B_d versus hysteresis $\theta_A - \theta_R$ for $\theta_A = 90°$, and for different optimal contact lines. Also shown are the shapes of the contact line as well as the drop profiles for $B_d = 0.4$. (*b*) As in (*a*) but for $\theta_A = 30°$. Contact line contours and drop profiles are shown for $B_d = 0.06$. Contact lines: ——, unconstrained; - - - -, *y*-constrained; – – –, circular.

range 10° to 90°. For the same value of hysteresis $\theta_A - \theta_R$, as the inclination angle decreases from 90°, the critical B_d increases. But for a drop on an inclined surface, the displacing force is not the total gravitational force or Bond number, but rather the tangential component of the gravitational force $B_T = B_d \sin\beta$. Figure 6 (*b*) shows the results of figure 6 (*a*) replotted with the ordinate axis showing the displacing force B_T. All the curves for several inclination angles β now fall close to the curve for $\beta = 90°$. At fixed B_T, we see that the inclination angle has only a very slight effect on the displacement condition. As β decreases from 90°, the normal component of gravitational force B_N increases, producing a slight spreading of the droplet over the surface. This increases the size of the contact line and increases the interfacial force, but yields only a marginal increase in the critical B_T for $10° \leqslant \beta \leqslant 90°$. For

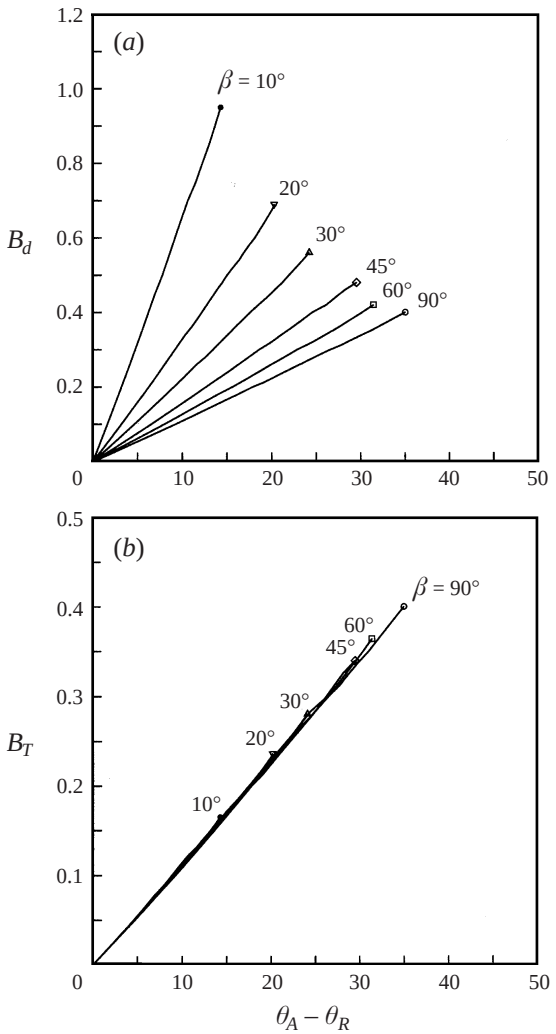

FIGURE 6. Influence of the inclination angle on the displacement of sessile droplets, for $\theta_A = 90°$ and for the unconstrained optimization problem. (*a*) Critical Bond number B_d versus hysteresis $\theta_A - \theta_R$. (*b*) Critical B_T versus hysteresis $\theta_A - \theta_R$.

asymptotically small angles β, the critical Bond number would become quite large, inducing significant spreading and producing a larger effect on the yield condition B_T.

To illustrate the effect of the normal force B_N on the droplets, we plot the optimal contact line contours and the drop profiles for $B_T = 0.225$ and for $\beta = 90°, 45°, 20°$ in figure 7 (*a*,*b*). Smaller inclination angles, or higher B_N, correspond to flatter drop shapes, which produces greater extension in both the x- and y-directions.

To show the difference between the unconstrained and the y-constrained shape, we plot in figure 8 three-dimensional views of a drop on an inclined wall with $\beta = 45°$ and $B_d = 0.4$ for these two optimal shapes. We see that the unconstrained shape shows the characteristic y-extension, while the y-constrained shape shows greater extension in the x-direction. These differences are also shown in the insets of figure 9, where we plot the critical force B_T versus hysteresis $\theta_A - \theta_R$ for $\beta = 45°$. As expected, for the same hysteresis, the critical force B_T is smaller for the y-constrained shape.

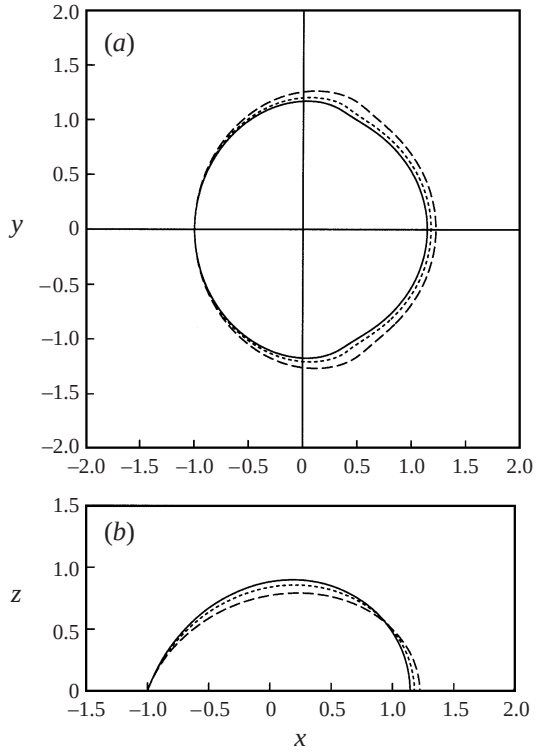

FIGURE 7. Influence of B_N on the shape of sessile droplets, for $\theta_A = 90^\circ$ and $B_T = 0.225$ for the unconstrained optimization problem. (*a*) The optimal shapes of the contact line. (*b*) Drop profiles. Inclination angle β: ——, 90°; - - - -, 45°; – – –, 20°.

3.3. *Displacement of a pendant drop*, $90^\circ \leqslant \beta \leqslant 180^\circ$

Having considered the influence of the inclination angle β on the displacement of droplets with a positive normal force, we now turn our attention to the displacement of pendant droplets ($90^\circ \leqslant \beta \leqslant 180^\circ$). As noted earlier, we assume that the drop density is higher than that of the surrounding fluid ($\rho_1 \geqslant \rho_2$); hence the normal force B_N now tends to pull the droplet away from the wall. In figure 10 we plot the critical B_T as a function of hysteresis $\theta_A - \theta_R$ for the unconstrained optimization problem and for several angles of inclination β in the range 90° to 178°.

For inclination angles in the range 90° to 160°, the results of this figure are similar to those for smaller inclination angles. In particular, we observe a weak dependence on the inclination angle with a monotonic dependence on the normal force component. As the force B_N increases, it pulls the droplet away from the wall, decreasing the radius of the contact line and weakening the interfacial force. This yields a slight reduction in the critical value of B_T.

For large angles β, the effect of the normal force is sufficiently large to have a qualitative effect on the equilibrium shapes. To illustrate this effect, we show detailed results for two characteristic cases $\beta = 160^\circ, 170^\circ$ in figures 11 and 12 respectively. In these figures, we observe the competing effects of the tangential and normal force components. For smaller inclination angles, the tangential force component is dominant and increasing Bond number lead to significant expansion of the contact line over the solid surface. For the $\beta = 160^\circ$ inclination shown in figure 11 (*a*),

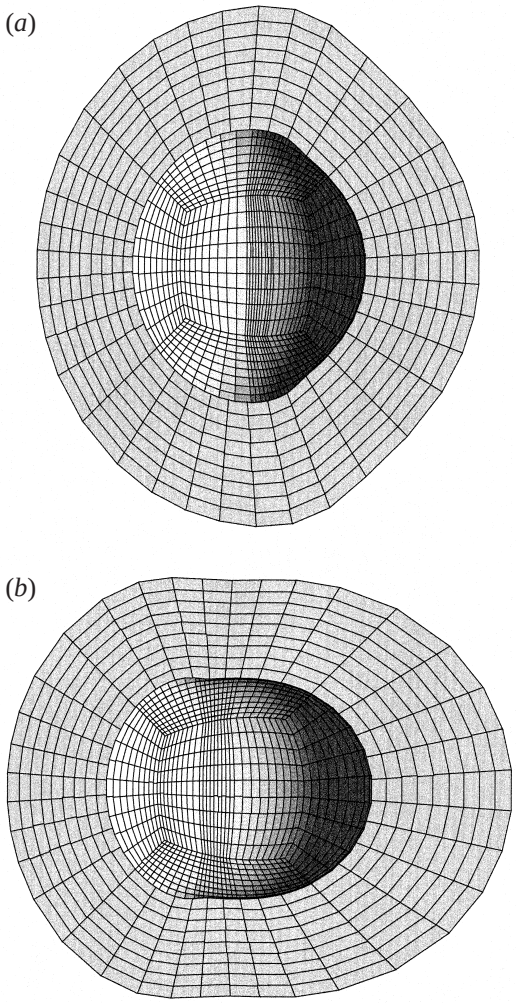

FIGURE 8. Equilibrium shapes for a sessile droplet with $\theta_A = 90^\circ$, for $\beta = 45^\circ$ and $B_d = 0.4$ (or $B_T = 0.283$). (*a*) The unconstrained optimal shape. (*b*) The y-constrained optimal shape.

the tangential and normal forces are nearly balanced, and the contact lines show minimal change as the Bond number is increased. For the $\beta = 170^\circ$ surface shown in figure 12(*a*), the normal force now dominates, and the contact line *contracts* with increasing Bond number. This contraction leads to a significant reduction in the critical value of B_T.

Additional results for pendant droplets including y-constrained optimizations are given in Dimitrakopoulos (1998).

3.4. *Displacement of a drop on a tiltable plane*

In § 3.1–§ 3.3, we studied the yield conditions for the gravitational displacement of a droplet on an inclined plane at fixed angle of inclination β while increasing the Bond number B_d. In this section, we keep the Bond number constant while increasing the angle of inclination. This problem corresponds to the procedure employed in many experiments on gravitational displacement. The question which arises is whether the

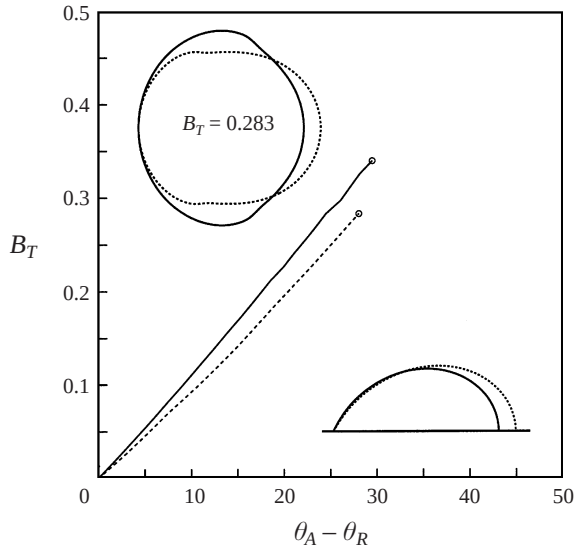

FIGURE 9. Critical B_T versus hysteresis $\theta_A - \theta_R$ for $\theta_A = 90°$ and $\beta = 45°$, for the unconstrained (——) and the y-constrained shape (- - - -) of the contact line. Also shown are the shapes of the contact line as well as the drop profiles for $B_d = 0.4$ (or $B_T = 0.283$).

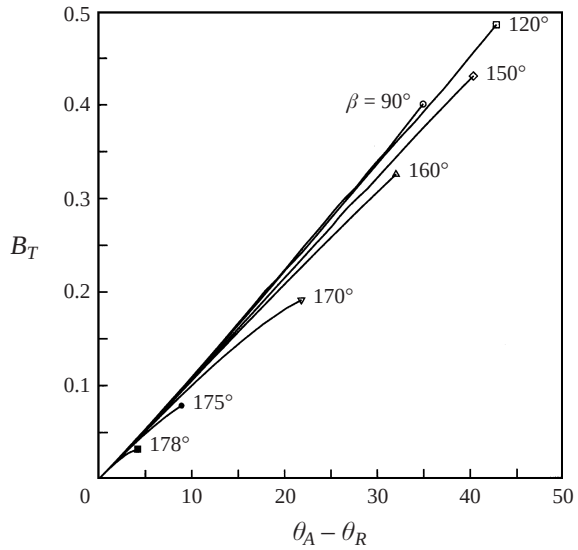

FIGURE 10. Influence of the inclination angle on the displacement of pendant droplets with advancing angle $\theta_A = 90°$, for the unconstrained optimization problem: critical B_T versus hysteresis $\theta_A - \theta_R$.

initial configuration and the conditions of the experiment affect the final value of the yield condition. For the unconstrained optimization, the predicted yield condition represents a true maximum independent of the initial configuration.

Thus none of the results for the unconstrained optimization are changed in the present section. For the y-constrained optimization however, the two different experimental procedures yield different initial configurations, and hence different y-constraints. In the previous subsections, the initial shape was that of a spherical

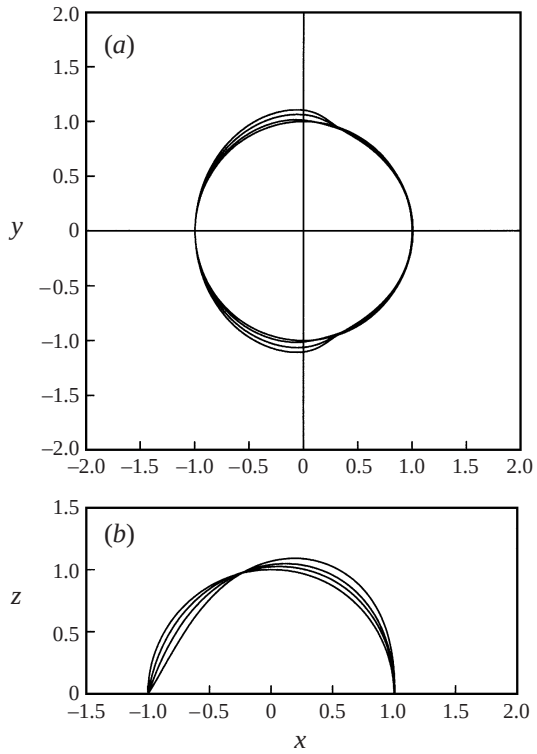

FIGURE 11 (*a–c*). For caption see facing page.

cap corresponding to $B_d = 0$. For the new model problem, we fix the Bond number and increase the inclination angle β from 0° to 90° (for sessile drops) or decrease β from 180° to 90° (for pendant drops). Therefore the undisturbed y-constrained shape corresponds to the equilibrium shape for the prescribed value of B_d at inclination of $\beta = 0°$ or $\beta = 180°$. Both shapes have circular contact lines, but the first shape is flatter than the spherical cap with a larger contact radius, while the second is taller and has a smaller contact radius.

We begin by considering the case of $0° \leqslant \beta \leqslant 90°$. Figure 13 shows the contact lines, drop profiles and three-dimensional views for the y-constrained optimization. The results of this figure may be compared with the analogous results shown in figure 4 for a vertical wall with increasing Bond number. Despite the differences in initial configurations, the behaviour of the droplets is quite similar in their response to the increased displacement force. For a quantitative comparison of the two different experiments, we may compare the yield condition in each system with the values predicted by the unconstrained optimization. The comparison for the present system is shown in figure 14 while the earlier results are presented in figure 5(*a*) for a vertical wall and in figure 9 for $\beta = 45°$. In all cases, the y-constrained optimization predicts a lower critical force B_T than the unconstrained optimization, but the relative magnitudes are similar in all cases.

We continue our study by considering the displacement of pendant droplets. For these droplets, the initial configuration is a droplet suspended from a horizontal surface with $\beta = 180°$. Figure 15 shows the results for the y-constrained optimization for a Bond number $B_d = 0.5$. The contact line contours and drop profiles for this

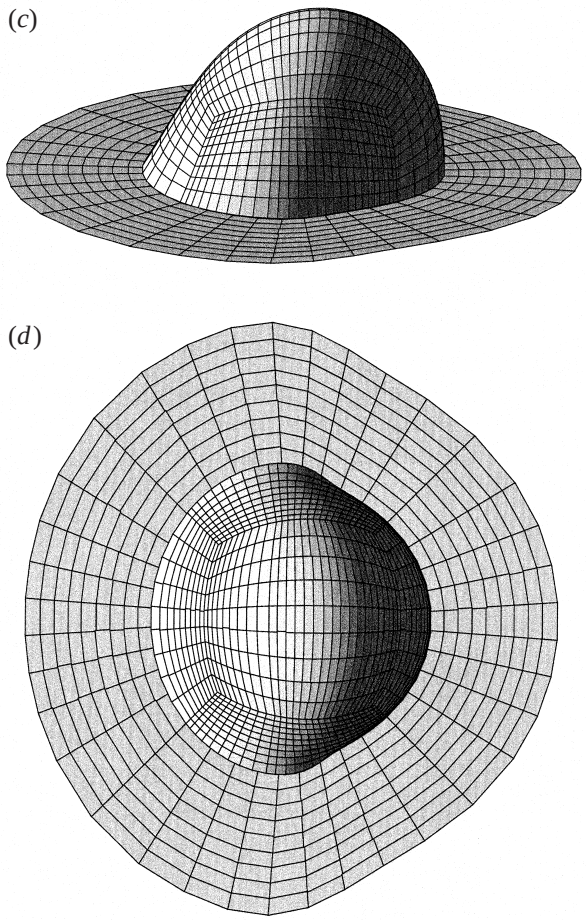

FIGURE 11. Equilibrium shapes for droplets with $\theta_A = 90^\circ$ on an inclined wall with $\beta = 160^\circ$ and for the unconstrained optimization problem. For (*a*,*b*) the Bond number is $B_d = 0$, 0.3, 0.6, 0.95. (*a*) The shape of the contact line. (*b*) The drop profile. (*c*,*d*) The drop surface for Bond number $B_d = 0.95$.

case closely resemble those for a vertical wall shown in figure 4. The curves in this figure do not show the contraction of contact lines previously seen for pendant drops at large β, because the initial configuration at $\beta = 180^\circ$ has already experienced the maximum contraction.

The critical force B_T for pendant droplets is plotted as a function of hysteresis $\theta_A - \theta_R$ in figure 16, for both the y-constrained and unconstrained optimizations. The insets show typical examples for the contact line contours and the drop profiles. As with the previous results, the critical B_T for the unconstrained optimization is proportionately higher than that for the y-constrained optimization.

To end this subsection, we collect results for the critical displacement force B_T for both sessile and pendant droplets and show the influence of the Bond number B_d in figure 17. This figure may be viewed as the complement of figures in earlier subsections which showed the influence of different β values while varying the Bond number. This figure illustrates the influence of the normal component of the gravitational force B_N. In particular, it shows a monotonic trend with the highest yield conditions

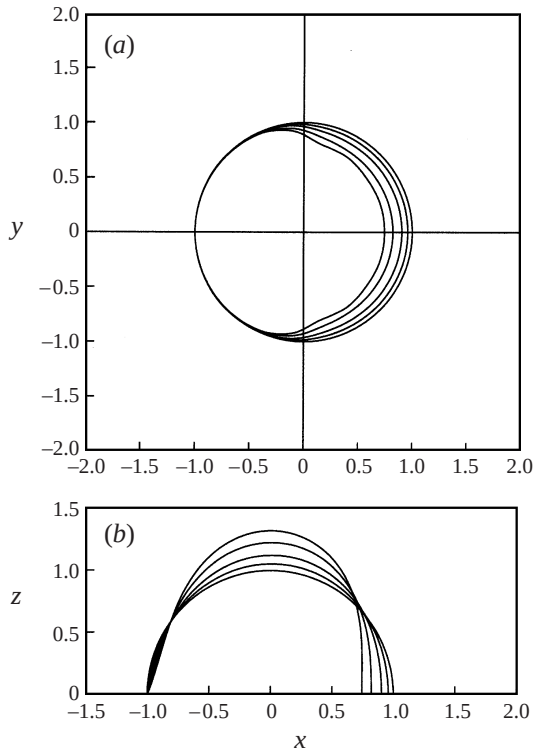

FIGURE 12. Equilibrium shapes for a droplet with $\theta_A = 90^\circ$ on an inclined wall with $\beta = 170^\circ$ and for the unconstrained optimization problem. The Bond number is $B_d = 0$, 0.3, 0.6, 0.9, 1.1. (*a*) The shape of the contact line. (*b*) The drop profile.

for the flattest droplets (sessile droplets, large B_d) and the lowest yield conditions for the tallest droplets (pendant droplets with large B_d). As noted earlier, this trend may be predicted from the connection between the width of the contact line and the total strength of the interfacial force.

3.5. *Comparison with experimental results and asymptotic theories*

In this subsection, we briefly consider some experimental observations and theoretical predictions which may be compared with the results of our computations. We note that there have been a number of observations of droplet shape for drops on inclined surfaces. Early efforts (Bikerman 1950; Furmidge 1962) reported symmetric oval shapes with parallel sides for *sliding* droplets, but Bikerman sketched an asymmetric profile for the droplet at the instant of incipient motion. Rotenberg *et al.* (1984) also show asymmetric profiles for attached drops. In a recent paper, Extrand & Kumagai (1995) observed the critical contact lines for droplets on inclined surfaces, and found curves which were neither circular, nor parallel sided, but exhibited asymmetric profiles consistent with the report of Bikerman. The asymmetric profiles reported in these papers compare well with our y-constrained profiles. In addition, Extrand & Kumagai (1995) provided a photograph of a water droplet on inclined PCTFE, at

FIGURE 13. Equilibrium shapes for a sessile droplet with $\theta_A = 90^\circ$ and $B_d = 0.5$, for the y-constrained optimization problem. For (*a*,*b*) the inclination angle is $\beta = 0^\circ$, 10°, 20°, 30°, 37.5°. (*a*) The shape of the contact line. (*b*) The drop profile. (*c*,*d*) The drop surface for $\beta = 37.5^\circ$.

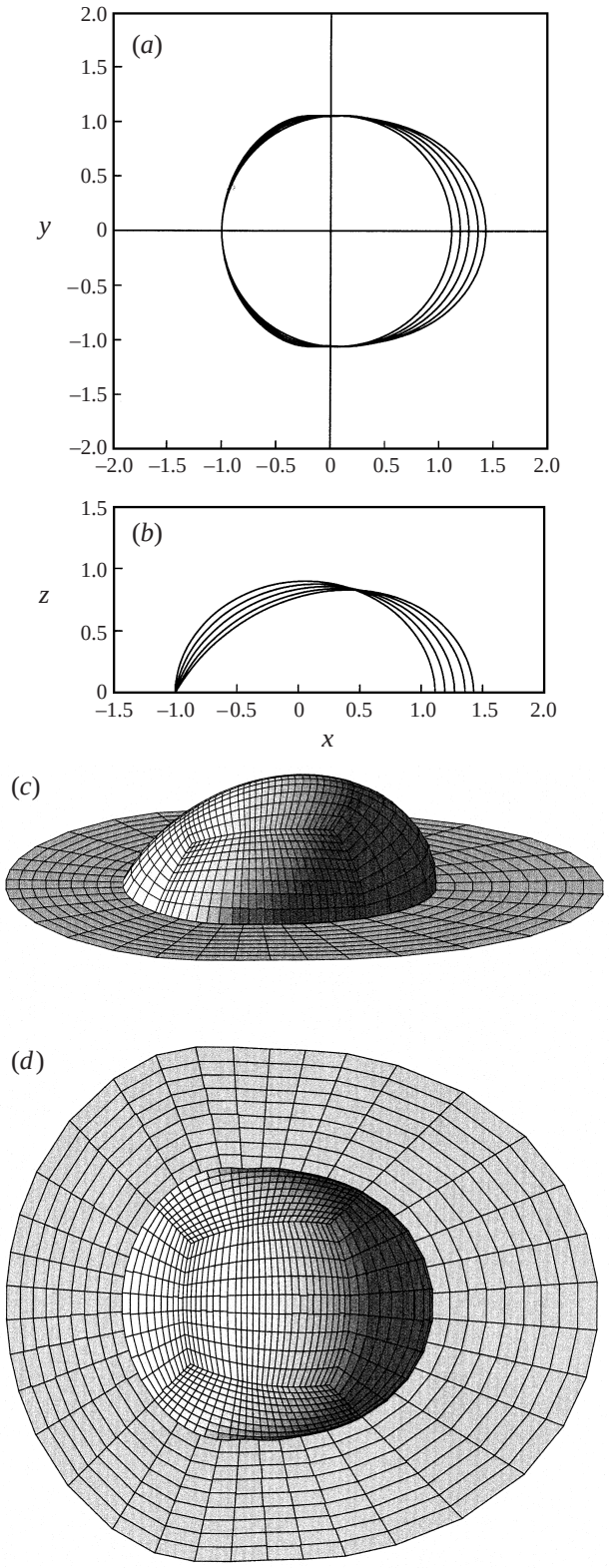

FIGURE 13. For caption see facing page.

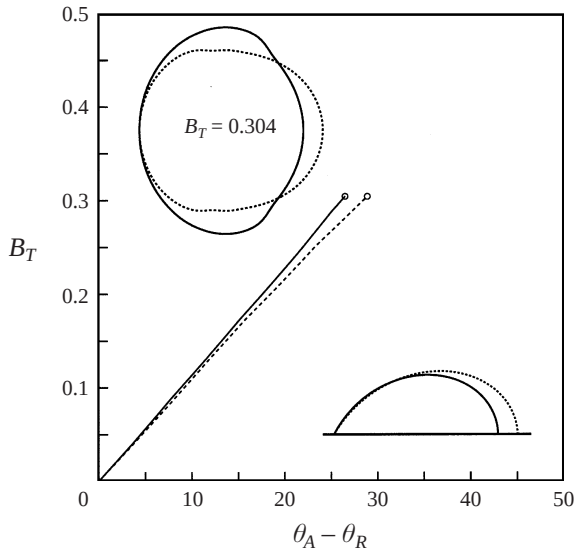

FIGURE 14. Critical B_T versus hysteresis $\theta_A - \theta_R$ for a sessile droplet with $\theta_A = 90^\circ$ and $B_d = 0.5$, for the unconstrained (——) and the y-constrained optimization problem (- - - -). Also shown are the contact line contours and the drop profiles for $\beta = 37.5^\circ$ (or $B_T = 0.304$).

the instant the drop began to move (their figure 3). In comparing this photograph with our y-constrained results for sessile droplets, we note that our predictions match the experiment in several key features including elongation, asymmetry and in the indentation and inflection points on the sides of the drop.

The prediction of the critical gravitational force for droplet displacement is probably the most important issue addressed in this paper. Unfortunately, the majority of experiments in the literature focus on the measurement of the contact angle hysteresis and do not provide detailed information of the yield conditions. Extrand & Kumagai (1998, personal communication) have provided details concerning their experiments including the Bond numbers and inclination angles for the onset of drop displacement. These data are plotted in figure 18 together with our predictions for y-constrained sessile droplets on a tiltable plane. The data are taken from experiments with water and ethylene glycol on a variety of different substrates. For each solid/liquid combination, measurements were taken for 3 or 4 different drop sizes yielding a different Bond number for each case. In all cases, the experimental data show a critical condition lower than that predicted by the numerical computations. For a given gravitational force B_T, the measured hysteresis $\theta_A - \theta_R$ ranges from 3° to 8° lower than the numerical prediction. The authors state that there is an uncertainty of as much as $\pm 3.4^\circ$ in the measured hysteresis; however this range does not quite explain the full deviation from our predictions.

There are two likely explanations for the discrepancy between the computations and the experimental data. First, we note the possibility that small amounts of surfactant might be present in the experimental system, reducing the surface tension

FIGURE 15. Equilibrium shapes for a pendant droplet with $\theta_A = 90^\circ$ and $B_d = 0.5$, for the y-constrained optimization problem. For (a,b) the inclination angle is $\beta = 180^\circ$, 170°, 160°, 150°, 140°, 130°. (a) The shape of the contact line. (b) The drop profile. (c,d) The drop surface for $\beta = 130^\circ$.

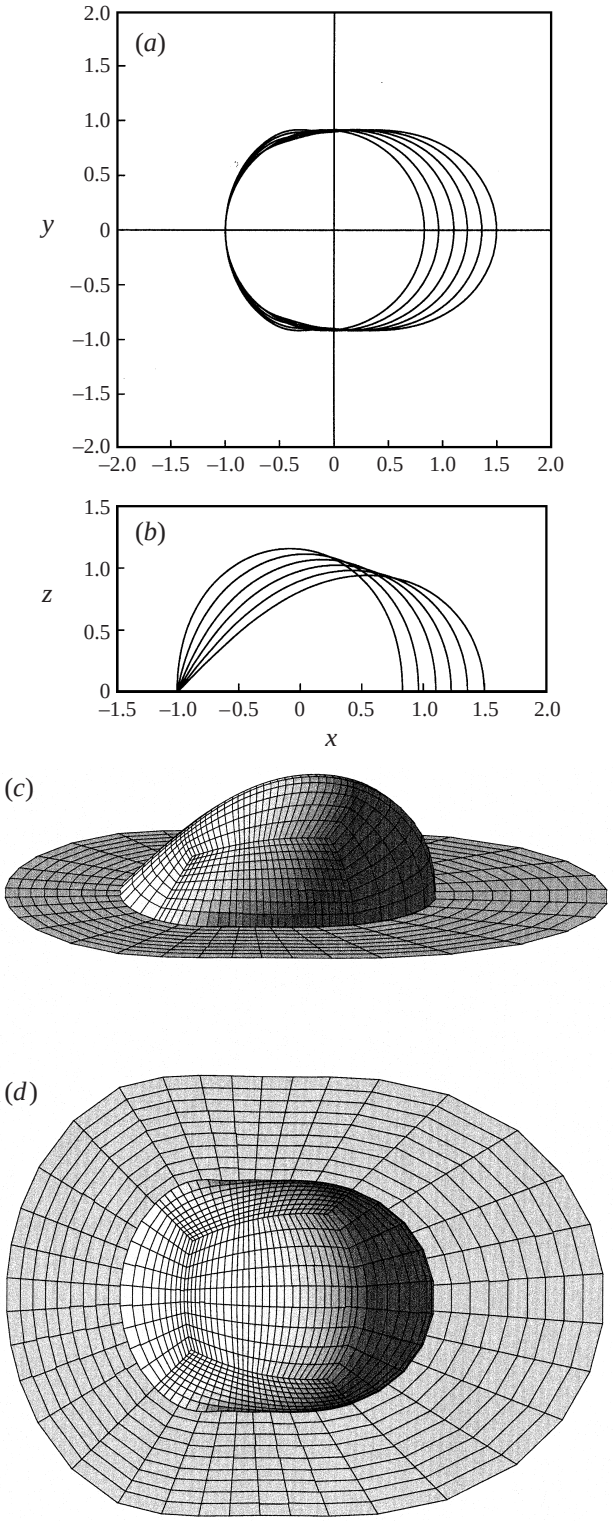

FIGURE 15. For caption see facing page.

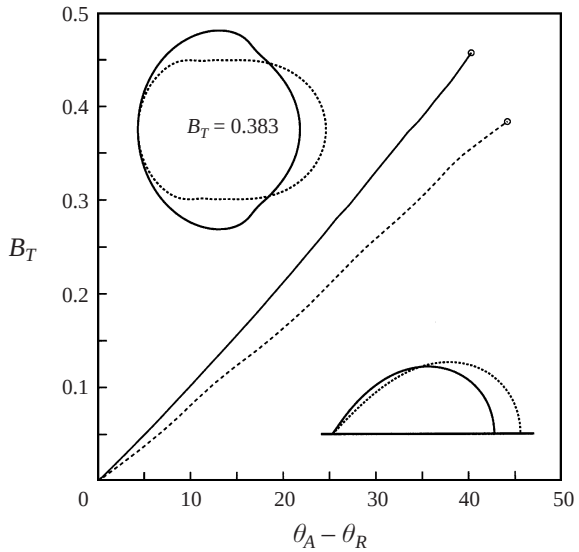

FIGURE 16. Critical B_T versus hysteresis $\theta_A - \theta_R$ for a pendant droplet with $\theta_A = 90^\circ$ and $B_d = 0.5$, for the unconstrained (——) and the y-constrained optimization problem (- - - -). Also shown are the contact line contours and the drop profiles for $\beta = 130^\circ$ (or $B_T = 0.383$).

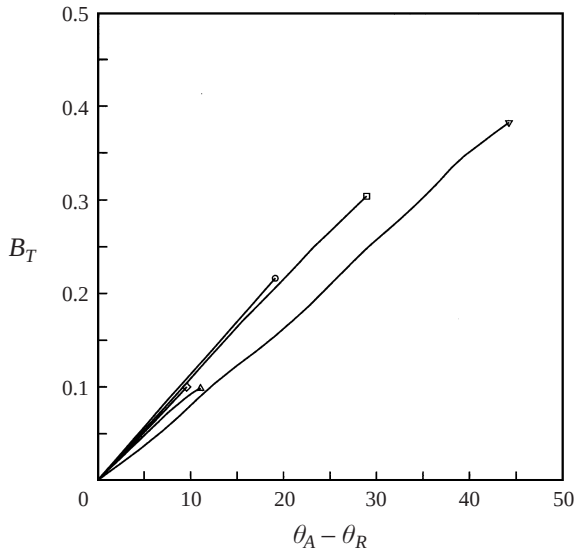

FIGURE 17. Critical B_T versus hysteresis $\theta_A - \theta_R$ for a droplet with $\theta_A = 90^\circ$ and for the y-constrained optimization problem. Sessile drop with B_d : ○, 1.0; □, 0.5; ◇, 0.1. Pendant drop with B_d: △, 0.1; ▽, 0.5.

and hence the measured yield force B_T. This effect would reduce the discrepancy with the numerical results. Second, we recall that the y-constrained predictions in the current effort derive from an *optimization* problem in which the drop contact line evolves from an initially circular shape to an elongated profile. In an experiment, there is no guarantee that the droplet will follow a path leading to this optimal configuration. As the inclination angle is increased, the droplet contact line may

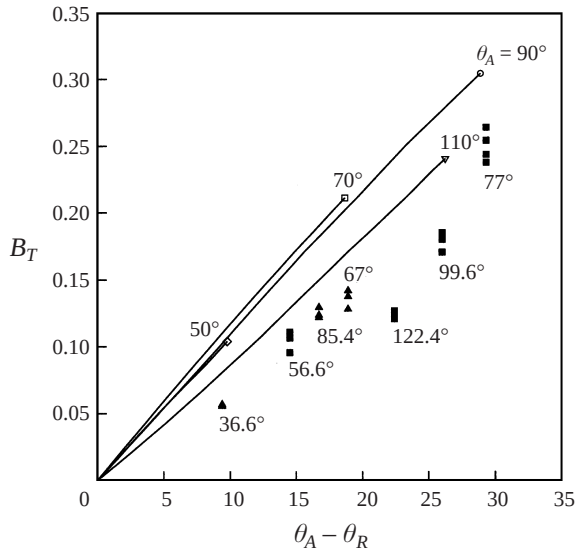

FIGURE 18. Comparison of our computational results to experimental data by Extrand & Kumagai (1995): critical B_T versus hysteresis $\theta_A - \theta_R$ for a sessile droplet on a tiltable plane. The solid lines represent our predictions for $B_d = 0.5$ and for the y-constrained optimization problem. Experimental data: ■, water; ▲, ethylene glycol; on several surfaces with Bond number B_d in the range of 0.57–1.24.

advance through a series of small discrete jumps. As the critical angle of inclination is approached, a small jump in the contact line may be sufficient to displace the droplet prematurely. Despite the quantitative discrepancies, we note that the experiments show good agreement with the computations in a number of qualitative trends. The data show an increase in displacement force with increasing hysteresis. In addition, the experimental data indicate a maximum slope for contact angles θ_A of 56.6°, 77° and 85.4° consistent with the predicted behaviour for θ_A. As noted above, the droplets also show qualitative agreement with the shape of the predicted contact lines.

Turning our attention to comparisons with previous computational efforts, we note that there have been no previous studies which predicted the shapes of the distorted contact lines. Brown *et al.* (1980) and Milinazzo & Shinbrot (1988) studied gravitational displacement assuming fixed circular contact lines. We have repeated our calculations using these assumptions and find excellent agreement with their results. The comparison between the optimal solutions and the circular contact lines has been discussed in the subsections above.

Theoretical predictions for the yield condition for gravitational displacement have been developed by Dussan V. & Chow (1983) and Dussan V. (1985) using asymptotic approximations. These authors assumed a droplet contour with an oval shape with parallel sides. They further assumed a constant angle θ_R on the front portion of the oval and a constant angle θ_A on the rear. These assumptions are broadly consistent with the results of our y-constrained optimization solutions.

In the first paper, Dussan V. & Chow employed small angle theory to determine the yield condition subject to the joint asymptotic limits $\theta_A - \theta_R \ll \theta_A \ll 1$. They provided a complicated expression for the yield condition which can be expanded into two expressions, one valid for $B_N \to 0$ and the other valid for $B_N \to \infty$. To compare with our results for a vertical wall with $\beta = 90°$ ($B_N = 0$), we consider the limit for

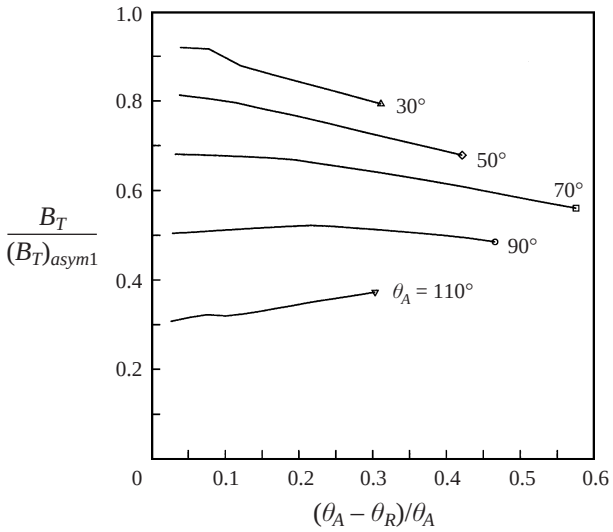

FIGURE 19. Ratio of critical B_T to asymptotic predictions based on (8) for $\beta = 90^\circ$ and for the y-constrained contact line.

$B_N \to 0$ and find

$$(B_T)_{asym1} = 0.8342\, \theta_A^{2/3}\, (\theta_A - \theta_R). \tag{8}$$

The predictions of the asymptotic theory are compared with the numerical computations for the y-constrained optimization in figure 19. Based on these results, we conclude that the quantitative predictions of the asymptotic theory are valid over a very limited range, with poor agreement with all direct numerical results of this paper. In fact, this is not surprising since Dussan V. & Chow's theory requires not only $\theta_A \ll 1$, but also $\theta_A - \theta_R \ll \theta_A$. Thus the theory is valid only for vanishingly small values of the contact angle hysteresis, i.e. only within a very small region in the upper left corner of figure 19. Despite its limited predictive range, the asymptotic theory is of significant interest, because it captures the correct physics and provides the proper scaling for small contact angles. Comparisons with the results for the unconstrained optimization problem and for other inclination angles appear similar to those in figure 19.

Dussan V. (1985) provided an asymptotic theory which is less restrictive and is valid for small contact angle hysteresis $\theta_A - \theta_R$ and Bond number B_d but for any advancing contact angle θ_A. While Dussan V.'s theory is based on a rigorous asymptotic analysis, the prediction for the yield condition for small hysteresis and Bond number reduces to a simple idealized model which is presented here.

For $B_d \ll 1$ and $\theta_A - \theta_R \ll 1$, the undisturbed droplet shape is a spherical cap with a circular contact line of radius r, which is connected with the characteristic radius a via the relation

$$V = \frac{4}{3}\pi a^3 = \frac{\pi}{3}\, \frac{r^3\, (2 - 3\cos\theta_A + \cos^3\theta_A)}{\sin^3\theta_A}. \tag{9}$$

In an idealized model, we may assume that the contact angle on the top half of the circle is equal to θ_R, while that on the bottom half is equal to θ_A. The total interfacial force on the droplet is then $F_\gamma = 2r\gamma(\cos\theta_R - \cos\theta_A)$. Substituting for r and setting the interfacial force equal to the gravitational force yields the prediction for the critical

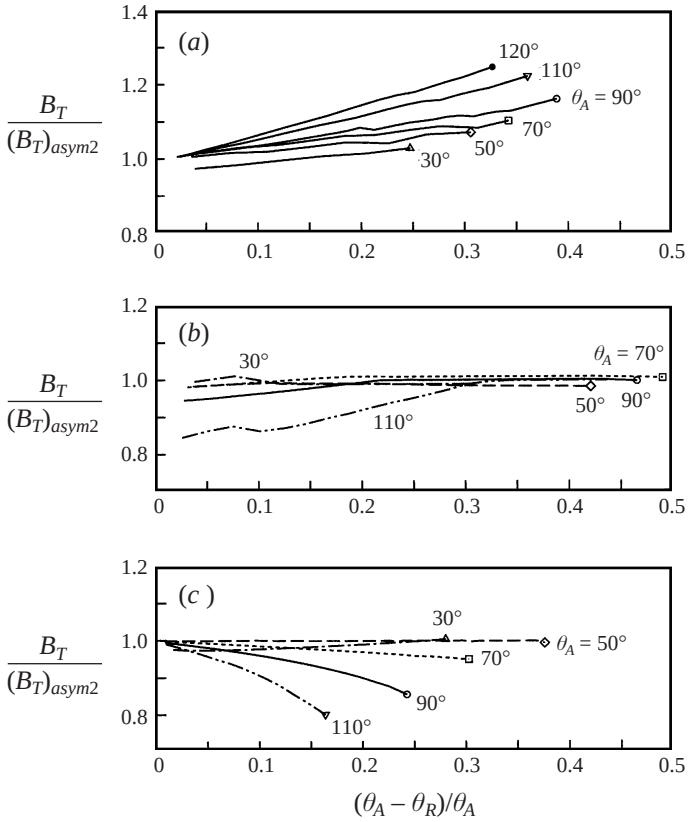

FIGURE 20. Ratio of critical B_T to asymptotic predictions based on (10). (*a*) Unconstrained optimal contact line and $\beta = 90^\circ$. (*b*) y-constrained contact line and $\beta = 90^\circ$. (*c*) Unconstrained optimal contact line and $\beta = 170^\circ$.

displacement force

$$(B_T)_{asym2} = \frac{3}{2^{1/3}\,\pi}\,\frac{(\cos\theta_R - \cos\theta_A)\,\sin\theta_A}{(2 - 3\cos\theta_A + \cos^3\theta_A)^{1/3}}. \tag{10}$$

This result is identical to Dussan V.'s (1985) asymptotic prediction in her equation (5.3).

In figure 20 we show the ratio of the numerical computations for B_T to the asymptotic prediction (10) as a function of the reduced hysteresis $(\theta_A - \theta_R)/\theta_A$. In these plots, the individual curves correspond to computations for different values of the advancing contact angle θ_A. Figure 20 (*a*,*b*) shows comparisons for unconstrained and y-constrained optimizations for vertical walls, while figure 20 (*c*) shows results for a pendant droplet with $\beta = 170^\circ$. The first conclusion is that all computed results show good agreement with the asymptotic theory in the limit as $\theta_A - \theta_R$ approaches zero. For the y-constrained optimization, the asymptotic theory shows good agreement for the entire range of $\theta_A - \theta_R$. While this may seem surprising at first, it can be explained by examining the contact lines and contact angle distributions in figure 4. While the droplet experiences significant elongation, the width of the droplet is unchanged, and the rapid change in the contact angle distribution is consistent with the assumption in the simple theory. Thus the idealized assumptions remain valid and the theory gives good predictions. By contrast, for the unconstrained optimization, the width of the

droplet increases significantly with increasing B_d, and the theory underpredicts the numerical results. For the pendant droplet at $\beta = 170^\circ$, the computed contact line contracts with increasing B_d for large contact angles, reducing the interfacial force, and decreasing the yield condition. In this case, the simple theory based on constant width overpredicts the critical displacement force. In summary, we find excellent agreement with the asymptotic theory in its range of validity, but see significant departures when the width of the contact line changes in response to the gravitational distortion.

4. Conclusions

In this paper we have conducted a comprehensive study of the problem of gravitational displacement for three-dimensional droplets from inclined solid surfaces. We have considered a wide selection of parameters to investigate the physical behaviour of different droplets and to test the limits of theoretical predictions. This study complements the analytical theories of Dussan V. & Chow (1983) and Dussan V. (1985). A number of important conclusions have been reached.

(i) The contact line contours for real droplets show fore-and-aft asymmetry with a distorted shape not well represented by the simple circular planforms assumed by previous authors. The distorted profiles allow rapid changes in contact angle which increases the ability of a droplet to stick to a surface. The y-constrained contact line contours predicted by our simulations show good qualitative agreement with experimental observations.

(ii) The critical gravitational force B_T predicted by the unconstrained optimization provides an upper bound on the yield condition for a droplet on an inclined surface. Alternative droplet configurations resulting from the y-constrained optimization show a small change in the predicted yield condition compared to the unconstrained case. Predictions based on circular contact lines show a significant change in the critical gravitational force.

(iii) Theoretical results based on small angle asymptotic theory give correct qualitative predictions; however, the range of applicability for accurate quantitative predictions is quite small. The critical B_T shows significant departure from the linear dependence on hysteresis $\theta_A - \theta_R$ predicted by the asymptotic theory of Dussan V. & Chow (1983). The analytical theory of Dussan V. (1985) gives correct quantitative predictions over a significant range outside its formal region of validity (i.e. for $\theta_A - \theta_R \ll 1$ and $B_d \ll 1$).

(iv) The normal component of the gravitational force B_N has a weak effect on the displacement of sessile droplets with stronger effect on the displacement of pendant droplets. The normal component B_N increases the critical displacement force B_T for a sessile droplet and decreases the critical B_T for a pendant droplet.

(v) The critical conditions for drop displacement are sensitive to the size of the contact angles. For a specified hysteresis $\theta_A - \theta_R$, increasing the contact angle θ_A increases the critical force B_T for values up to $\theta_A \approx 70^\circ$ and decreases the critical force for higher values of θ_A.

This work was supported by the National Science Foundation. Panagiotis Dimitrakopoulos acknowledges the support of the H. G. Drickamer Fellowship in the Department of Chemical Engineering. Computations were performed on IBM RISC6000 workstations furnished with support from the IBM SUR program at the University

of Illinois as well as on multiprocessor computers provided by the National Center for Supercomputing Applications.

REFERENCES

BIKERMAN, J. J. 1950 Sliding of drops from surfaces of different roughnesses. *J. Colloid Sci.* **5**, 349–358.

BROWN, R. A., ORR JR., F. M. & SCRIVEN, L. E. 1980 Static drop on an inclined plate: analysis by the finite element method. *J. Colloid Interface Sci.* **73**, 76–87.

DIMITRAKOPOULOS, P. 1998 Displacement of fluid droplets from solid surfaces. PhD thesis, University of Illinois.

DIMITRAKOPOULOS, P. & HIGDON, J. J. L. 1997 Displacement of fluid droplets from solid surfaces in low-Reynolds-number shear flows. *J. Fluid Mech.* **336**, 351–378 (referred to herein as DH1).

DIMITRAKOPOULOS, P. & HIGDON, J. J. L. 1998 On the displacement of three-dimensional fluid droplets from solid surfaces in low-Reynolds-number shear flows. *J. Fluid Mech.* **377**, 189–222 (referred to herein as DH2).

DUSSAN V., E. B. 1985 On the ability of drops or bubbles to stick to non-horizontal surfaces of solids. Part 2. Small drops or bubbles having contact angles of arbitrary size. *J. Fluid Mech.* **151**, 1–20.

DUSSAN V., E. B. & CHOW, R. T.-P. 1983 On the ability of drops or bubbles to stick to non-horizontal surfaces of solids. *J. Fluid Mech.* **137**, 1–29.

EXTRAND, C. W. & KUMAGAI, Y. 1995 Liquid drops on an inclined plane: the relation between contact angles, drop shape, and retentive force. *J. Colloid Interface Sci.* **170**, 515–521.

FURMIDGE, C. G. L. 1962 Studies at Phase Interfaces: The sliding of liquid drops on solid surfaces and a theory for spray retention. *J. Colloid Sci.* **17**, 309–324.

GOOD, R. J. 1979 Contact angles and the surface free energy of solids. In *Surface and Colloid Science* (ed. R. J. Good & R. R. Stromberg). Plenum, London.

GOOD, R. J. & KOO, M. N. 1979 The effect of drop size on contact angle. *J. Colloid Interface Sci.* **71**, 283–292.

MILINAZZO, F. & SHINBROT, M. 1988 A numerical study of a drop on a vertical wall. *J. Colloid Interface Sci.* **121**, 254–264.

ROTENBERG, Y., BORUVKA, L. & NEUMANN, A. W. 1984 The shape of nonaxisymmetric drops on inclined planar surfaces. *J. Colloid Interface Sci.* **102**, 424–434.

TUCK, E. O. & SCHWARTZ, L. W. 1991 Thin static drops with a free attachment boundary. *J. Fluid Mech.* **223**, 313–324.